Nanoscale

PAPER

View Article Online
View Journal | View Issue

Cite this: *Nanoscale*, 2014, **6**, 6844

Self-assembly of 21-arm star-like diblock copolymer in bulk and under cylindrical confinement

Yuci Xu,[ab] Weihua Li,*[c] Feng Qiu[c] and Zhiqun Lin*[b]

Received 8th March 2014
Accepted 11th April 2014

DOI: 10.1039/c4nr01275e

www.rsc.org/nanoscale

Phase behaviors of a 21-arm star-like diblock copolymer in bulk and under confinement were explored by using the pseudo-spectral method of a self-consistent mean field theory. An asymmetrical phase diagram in bulk was constructed by comparing the free energy of different structures. The gyroid phase was found to possess a large phase region when the inner block in the star-like diblock copolymer has a small volume fraction, suggesting the propensity to form the gyroid phase under this condition. Combined with the early experimental work, a scaling law correlating the period of lamellae $D_{multiarms}$ formed from multi-arm star-like block copolymers with the number of arms f was identified, that is, $D_{multiarms} = D/f^{1/2}$, where D is the period of a linear diblock copolymer with the same degree of polymerization N as a star-like diblock copolymer. The scaling law was also substantiated by the scaling theory. The bridging fraction of the lamellae formed in a star-like diblock copolymer was nearly 100%, which is advantageous for improving its mechanical properties. Some interesting two-dimensional and three-dimensional morphologies were yielded under the cylindrical confinement, where a 3D double helix was found to be the most stable structure.

Introduction

Star-like block copolymers have garnered considerable attention over the past decades because their unique solution and solid-state properties make them attractive candidates for potential applications in additives, coatings, drug delivery, and supramolecular science.[1–4] The order-disorder phase transition (ODT) of graft and star copolymers can be theoretically calculated[5] by using the random phase approximation (RPA) method.[6] For the A_fB_f star copolymer where all A and B blocks are connected to a common core, there is a critical point at $(\chi N)_c = 10.5$ for all values of f at the volume fraction $\phi = 0.50$, where χ is the Flory–Huggins interaction parameter, signifying the interaction between A and B blocks, and N is the degree of polymerization of the A_fB_f star copolymer. However, for the f-arm star-like block copolymer $(AB)_f$, where A and B refer to the inner and outer blocks, respectively, there is no critical point. The spinodal values $(\chi N)_s$ in this copolymer are equal to 8.86, 7.07, 5.32, and 4.33 for $f = 2$, 4, 10 and 30, respectively, at $\phi = 0.5$.[5] It is worth noting that RPA can only calculate the ODT of block copolymers, including linear and non-linear architectures. For the order–order phase transition (OOT), the self-consistent mean field theory (SCMFT) is needed to obtain the free energy of the molten block copolymers (both linear and non-linear block copolymers).[7] A powerful spectral method of SCMFT for solving the modified diffusion equation was developed,[8,9] with which the OOT can be readily calculated, and thus the phase diagram of star-like block copolymers with 1, 3, 5, and 9 arms were successfully constructed.[9] Notably, for the 9-arm star-like block copolymer, the phase region of gyroid and O^{70} phases was found to be larger than that in a linear diblock copolymer, and the phase diagram of the star-like block copolymer was asymmetric. In addition to the SCMFT, the dissipative particle dynamics (DPD) simulation was also carried out to investigate the microphase separation of two types of star-like diblock copolymers, *i.e.*, A_4B_4 and $(AB)_4$.[10] A series of nanostructures, including lamellae, perforated lamellae, cylinders and body-centered-cubic spheres, and gyroid, were identified. The phase diagrams of these two star-like diblock copolymers were different. For the A_4B_4, the phase diagram was symmetric, while an asymmetric phase diagram was yielded for the $(AB)_4$, which was consistent with the SCMFT results.

$(AB)_f$ type star-like diblock copolymers were synthesized by the copolymerization of polystyrene-*block*-polyisoprene (PS-*b*-PI) anions with divinylbenzene (DVB) initiated by *n*-butyllithium.[11] The number of arms f can be controlled by the

[a]*Department of Macromolecular Science and Engineering, Faculty of Materials Science and Chemical Engineering, Ningbo University, Ningbo, Zhejiang 315211, China*

[b]*School of Materials Science and Engineering, Georgia Institute of Technology, Atlanta, Georgia 30332, USA. E-mail: zhiqun.lin@mse.gatech.edu*

[c]*State Key Laboratory of Molecular Engineering of Polymer, Key Laboratory of Computational Physical Science, Ministry of Education, Department of Macromolecular Science, Fudan University, Shanghai 200433, China. E-mail: weihuali@fudan.edu.cn*

concentration of diblock anion or the feed ratio of DVB to the diblock anion end.[11] The period of lamellae formed in the $(AB)_f$ star-like copolymer ($f < 77$) were found to be the same as those of the corresponding diblock arms.[11] Recently, 21-arm, star-like block copolymers, including coil–coil poly(acrylic acid)-*b*-polystyrene (PS-*b*-PAA) and coli-rod poly(acrylic acid)-*b*-poly(3-hexylthiophene) (PAA-*b*-P3HT), have been synthesized by sequential atom transfer radical polymerization (ATRP)[12] and a combination of click chemistry with living polymerization.[13] All diblock copolymer arms were grown from the β-cyclodextrin (β-CD) core.[12,13] These intriguing star-like block copolymers can be utilized as nanoreactors to craft a wide range of functional nanoparticles (*e.g.*, metallic, ferroelectric, magnetic, luminescent, semiconductor, *etc.*) with well-controlled dimension and solubility. The inner PAA block in 21-arm star-like block copolymers is hydrophilic and facilitates the precursors to be preferentially incorporated into the interior space occupied by PAA blocks through a strong coordination bonding between the carboxyl groups of PAA and the metal moiety of precursors, yielding nanoparticles that are intimately and permanently tethered with the outer block of star-like block copolymers (*e.g.*, PS).[14] We note that there is no study on the phase behavior of 21-arm star-like block copolymers, especially the effect of the star-like architecture on the phase behavior. Moreover, in comparison to linear diblock copolymers, the bridge fraction of the morphologies formed from 21-arm star-like block copolymers is expected to be much higher due to a large number of arms. Accordingly, the mechanical properties of materials built upon them would be largely improved for use in thermoplastic elastomers.[15]

Herein, we report the self-assembly of 21-arm star-like diblock copolymers [denote star-like $(AB)_{21}$, where A and B are the inner and outer blocks, respectively] in bulk and under cylindrical confinement. The pseudo-spectral method of SCMFT was employed to calculate the free energy and the periods of different morphologies. The equilibrium ordered phases determined by the molecular composition and architecture can be explored by using this powerful theoretical framework. Once the solutions of the SCMFT equations corresponding to the morphologies are obtained, an asymmetric phase diagram of 21-arm star-like diblock copolymers can then be constructed by comparing the free energy of phases, and the period of morphologies can also be determined during the minimization of free energy. The gyroid phase was found to exhibit a large phase region when the inner block in a star-like diblock copolymer has a small volume fraction, suggesting the propensity to form the gyroid phase under this condition. The distributions of the core that connect each AB arm together, the chain end of B blocks, and the junction point between A and B blocks were calculated. The bridging fraction of the lamellae formed in the star-like diblock copolymer was nearly 100%, which is highly desirable for improving its mechanical properties. When subjecting to the cylindrical confinement, several interesting two-dimensional and three-dimensional morphologies were found, where a 3D double helix was observed to be the most stable structure.

Theory

In this study, a system consisting of incompressible melts of a star-like, coil–coil $(AB)_f$ diblock copolymer is considered, where f is the number of arms ($f = 21$ for a 21-arm star-like diblock copolymer). A and B blocks are the inner and outer blocks, respectively, in the star-like $(AB)_f$ diblock copolymer. Each star-like polymer has an equal degree of polymerization N and the degree of polymerization of each arm is N/f. The volume fractions of A blocks and B blocks, ϕ_A and ϕ_B, are defined as N_A/N and N_B/N, respectively, where N_A and N_B are the degree of polymerization of A blocks and B blocks in the star-like diblock copolymer, respectively. The interaction between two dissimilar polymers is characterized by Flory–Huggins interaction parameter χ. The length in SCMFT is expressed in the units of the radius of gyration of linear polymer, $R_g = (Nb^2/6)^{1/2}$, where b is the Kuhn length. According to many-chain Edwards theory,[16–19] the free energy functional F for a number of n Gaussian 21-arm star-like diblock copolymer chains in bulk and under cylindrical confinement are

$$\frac{F}{nk_BT} = -\ln Q + \frac{1}{V}\int d\mathbf{r}\{\chi N\phi_A(\mathbf{r})\phi_B(\mathbf{r}) - \omega_A(\mathbf{r})\phi_A(\mathbf{r}) - \omega_B(\mathbf{r})\phi_B(\mathbf{r}) - \eta(\mathbf{r})[1 - \phi_A(\mathbf{r}) - \phi_B(\mathbf{r})]\} \quad (1)$$

and

$$\frac{F}{nk_BT} = -\ln Q + \frac{1}{V}\int d\mathbf{r}\{\chi N\phi_A(\mathbf{r})\phi_B(\mathbf{r}) - \omega_A(\mathbf{r})\phi_A(\mathbf{r}) - \omega_B(\mathbf{r})\phi_B(\mathbf{r}) - \eta(\mathbf{r})[1 - \phi_A(\mathbf{r}) - \phi_B(\mathbf{r})] + H(\mathbf{r})[\phi_A(\mathbf{r}) - \phi_B(\mathbf{r})]\} \quad (2)$$

respectively, where $\phi_A(\mathbf{r})$ and $\phi_B(\mathbf{r})$ are the monomer densities of A and B blocks, respectively. Q is the partition function of a single polymer (*i.e.*, a star-like diblock copolymer in the present study) interacting with the mean fields ω_A and ω_B produced by the surrounding chains. For the confined melts, the spatial integration is restricted to the pore volume V. A surface field in eqn (2) is introduced to characterize the preference of the pore wall to different blocks. Similar to our previous work,[20–23] this surface field is chosen to have the following form

$$\frac{H(\mathbf{r})}{\chi N} = V_0\{\exp[(\sigma + |\mathbf{r}| - R)/\lambda] - 1\} \quad (3)$$

for $R - \sigma \le |\mathbf{r}| \le R$, while $H(\mathbf{r}) = 0$ for $|\mathbf{r}| < R - \sigma$. In this work, the distance of the surface interaction is chosen as $\sigma = 0.5R_g$, and the decay length λ equals 0.5 R_g. $V_0 = 0$ implies that there is no preferential interaction between the pore and the A (or B) block. The pore wall prefers the inner A block at $V_0 < 0$ and prefers the outer B block at $V_0 > 0$.

The minimization of the free energy with respect to the monomer densities and the mean fields leads to the following standard mean-field equations for copolymer in bulk and under confinement, respectively.

$$\omega_A(\mathbf{r}) = \chi N\phi_B(\mathbf{r}) + \eta(\mathbf{r})$$
$$\omega_B(\mathbf{r}) = \chi N\phi_A(\mathbf{r}) + \eta(\mathbf{r})$$
$$\phi_A(\mathbf{r}) + \phi_B(\mathbf{r}) = 1$$
$$\phi_A(\mathbf{r}) = \frac{1}{Q}\int_{s\in A} ds q_A(\mathbf{r},s)q_A^\dagger(\mathbf{r},s)$$
$$\phi_B(\mathbf{r}) = \frac{1}{Q}\int_{s\in B} ds q_B(\mathbf{r},s)q_B^\dagger(\mathbf{r},s) \quad (4)$$
$$Q = \frac{1}{V}\int d\mathbf{r} q_K(\mathbf{r},s)q_K^\dagger(\mathbf{r},s)$$

and

$$\omega_A(\mathbf{r}) = \chi N\phi_B(\mathbf{r}) + H(\mathbf{r}) + \eta(\mathbf{r})$$
$$\omega_B(\mathbf{r}) = \chi N\phi_A(\mathbf{r}) - H(\mathbf{r}) + \eta(\mathbf{r})$$
$$\phi_A(\mathbf{r}) + \phi_B(\mathbf{r}) = 1$$
$$\phi_A(\mathbf{r}) = \frac{1}{Q}\int_{s\in A} ds q_A(\mathbf{r},s)q_A^\dagger(\mathbf{r},s)$$
$$\phi_B(\mathbf{r}) = \frac{1}{Q}\int_{s\in B} ds q_B(\mathbf{r},s)q_B^\dagger(\mathbf{r},s) \quad (5)$$
$$Q = \frac{1}{V}\int d\mathbf{r} q_K(\mathbf{r},s)q_K^\dagger(\mathbf{r},s)$$

In the equations noted above, $q_K(\mathbf{r}, s)$ and $q_K^\dagger(\mathbf{r}, s)$ ($K = A, B$) are the end-segment distribution functions, which are proportional to the probability that a polymer segment, of contour length s and with one free end, has its other end located at $\mathbf{r}$. These distribution functions satisfy the modified diffusion equations.

$$\frac{\partial q_K(\mathbf{r},s)}{\partial s} = \nabla^2 q_K(\mathbf{r},s) - \omega_K(\mathbf{r})q_K(\mathbf{r},s)$$
$$-\frac{\partial q_K^\dagger(\mathbf{r},s)}{\partial s} = \nabla^2 q_K^\dagger(\mathbf{r},s) - \omega_K(\mathbf{r})q_K^\dagger(\mathbf{r},s) \quad (6)$$

The initial conditions are $q_B^\dagger(\mathbf{r}, 1) = 1$, $q_A(\mathbf{r}, 0) = [q_A^\dagger(\mathbf{r}, 0)]^{f-1}$. The split-step Fourier method was employed to solve the modified diffusion equations for the end-segment distribution functions.[24,25] Similar to our previous work on the block copolymers under the confinement,[20–22] the cross section of the pore is placed in a rectangular cell, which is a little larger than the pore diameter. The periodic boundary conditions are imposed automatically on the square cell in the split-step Fourier method. The cell is discretized into $N_x \times N_y = 64 \times 64$ and $N_x \times N_y \times N_z = 64 \times 64 \times 64$ for 2D and 3D, respectively, which is reliable to give accurate results according to our previous work.[20] The total chain contour (N_s) is divided into 1000 segments. We note that in the current system, the phase transition points of the system are found to be insensitive to the variation in Ns from 1000 (transition point: $\chi N = 170$, $\phi_A = 0.17778$) to 2000 (transition point: $\chi N = 170$, $\phi_A = 0.17768$), suggesting that 1000 segments are sufficient to produce an accurate phase diagram.

Results and discussion

Period of the lamellar structure

The radius of gyration of a multi-arm star-like block copolymer ($R_{g\_Multiarm}$) can be written as follows:[26]

$$\left\langle R_g^2 \right\rangle_{Multiarm} = \frac{Nb^2}{6}\left(\frac{3-2/f}{f}\right) = \left(\frac{3-2/f}{f}\right)\left\langle R_g^2 \right\rangle_{Linear} \quad (7)$$

where N is the total degree of polymerization of a star-like block copolymer and f is the number of arms. Clearly, $R_{g\_Multiarm}$ decreases as f increases at the fixed N, and it is smaller than that of a linear diblock copolymer with the same N. As a result, the characteristic distance (*i.e.*, period) of the structures formed from the multi-arm star-like diblock copolymer is anticipated to be smaller than that of a linear diblock copolymer.

As the lamellar structure is one of the most common nanostructures seen in diblock copolymers, the period of this morphology was first investigated. We fixed $\chi N/f = 13.33$ and $\phi_A = 0.5$. The periods in SCMFT are normalized with respect to the radius of gyration of linear polymer, $R_g = (Nb^2/6)^{1/2}$. The variation of the period of lamellae as a function of f is shown in Fig. 1. For the squares, the period decreases with the increase in f at the fixed N; this is obvious as the increase of f leads to the decrease of N/f (*i.e.*, the degree of polymerization of each arm). Additionally, there is a scaling law correlating the period of a star-like diblock copolymer, $D_{multiarms}$ to f, that is, $D_{multiarms} = D/f^{1/2}$, where D is the period of linear a diblock copolymer with the same N. The circles are the estimated values from the scaling law. Obviously, the scaling relationship can be established as the squares and circles overlap one another.

On the other hand, when the degree of polymerization of each arm (*i.e.*, N/f) for different number of arms f is fixed, the period of $(AB)_f$ would be the same as that of a linear diblock copolymer, as clearly evidenced in Fig. 1 (triangles). It is interesting to note that this calculated result is in good agreement with the experimental observation in which the characteristic distance of star copolymers was the same as that of the

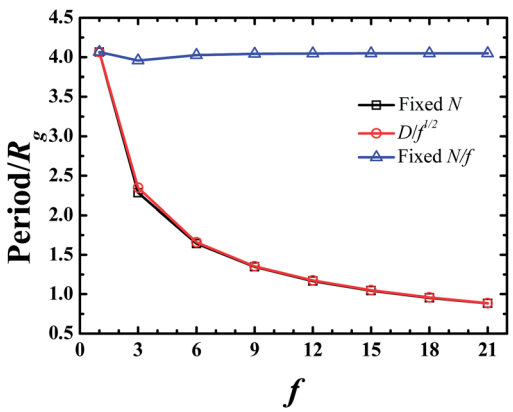

Fig. 1 Lamellar periods of different multi-arm star-like diblock copolymers as a function of the number of arms, f at the fixed N (squares) and N/f (triangles), respectively, at $\chi N/f = 13.33$ and $\phi_A = 0.5$. The circles represent the estimated periods by the scaling law, $D/f^{1/2}$, where D is the period of a linear diblock copolymer with the same N.

corresponding linear diblock copolymers.[11] On the basis of the results noted above, the following relationship between f and $D_{\text{multiarms}}$ can be easily obtained.

$$D_{\text{multiarms}} = D/f^{1/2} \text{ at the fixed } N \quad (8)$$

$$D_{\text{multiarms}} = D \text{ at the fixed } N/f \quad (9)$$

Notably, the degree of polymerization of the corresponding linear diblock copolymer in eqn (8) is N, while it is N/f in eqn (9). These two equations can also be corroborated by the scaling theory discussed below.

Scaling theory

In this section, a simple scaling theory can be used to account for the relationship between the period, both D and $D_{\text{multiarms}}$, and the number of arms, f. Considering the simple lamellae morphology in the star-like diblock copolymer $(AB)_f$, the framework of strong segregation theory (SST)[27] can be applied to describe this system. A and B chains form two brushes with the heights of $h_{A.0}$ and $h_{B.0}$, respectively.

$$h_{A.0} = \frac{\phi Nn}{fA\rho_0} = \frac{\phi N}{f\Sigma\rho_0} \quad (10)$$

$$h_{B.0} = \frac{(1-\phi)Nn}{fA\rho_0} = \frac{(1-\phi)N}{f\Sigma\rho_0} \quad (11)$$

$$D_{\text{multiarms}} = 2 \times (h_{A.0} + h_{B.0}) = \frac{2N}{f\Sigma\rho_0} \quad (12)$$

where Σ is the interfacial area per molecule, $\Sigma \equiv A/n$, and ρ_0 is the segment density.

According to the free energy of the lamellae-forming linear diblock copolymer,[28] the free energy (F) of a star-like diblock copolymer with a lamellae morphology can be written as:

$$\frac{F}{nk_BT} \sim \Sigma\rho_0 b\left(\frac{\chi}{6}\right)^{1/2} + \frac{(D_{\text{multiarms}}/2)^2}{(N/f)b^2} \quad (13)$$

$$\sim \frac{2N}{D_{\text{multiarms}}f} b\left(\frac{\chi}{6}\right)^{1/2} + \frac{(D_{\text{multiarms}}/2)^2}{(N/f)b^2} \quad (14)$$

The first term is the interfacial free energy.[28] The second term, representing the total stretching energy, is obtained from the free energy of the ideal chain. The interfacial energy term favors the large $D_{\text{multiarms}}$ by decreasing the interfacial area, while the stretching term prefers the small $D_{\text{multiarms}}$. Thus, the equilibrium period can be identified by the minimization of F with respect to $D_{\text{multiarms}}$:

$$D_{\text{multiarms}} \sim 2^{2/3}(N/f)^{1/2} b\left(\frac{\chi N}{6f}\right)^{1/6} \quad (15)$$

$$D \sim 2^{2/3}(N)^{1/2} b\left(\frac{\chi N}{6}\right)^{1/6} \quad \text{when } f = 1 \quad (16)$$

When $\chi N/f$ is fixed, the scaling law can be determined: $D_{\text{multiarms}} = D/f^{1/2}$. While at the fixed N/f, it shows $D_{\text{multiarms}} = D$. These findings agree well with those obtained using SCFT as well as the experimental observations.[11] We note that for the periods of other complex structures, including cylinders, gyroids, and spheres, because of the effect of the spontaneous curvature, the relationships between D and f are more complex. Moreover, due to the nature of star-like architecture, the period between the normal (where the outer B blocks form the matrix) and the inverse (where the inner A blocks constitute the matrix) structures would be different. Nonetheless, we will not discuss them much as the present work focuses on the phase behavior of a 21-arm star-like diblock copolymer.

Distributions of some special segments

In the following text, we focus on the cylinder morphology formed in a 21-arm star-like diblock copolymer. There are two types of cylindrical phases. In the first type, the cylinder is composed of the inner A blocks, while the outer B blocks form the matrix. Fig. 2a shows the density distribution of A block of a typical cylindrical phase, which is denoted C (normal cylindrical phase). The second type of cylinders is shown in Fig. 3a, which is designated as $\bar{C}$ (inverse cylindrical phase), indicating that the cylinders comprise the outer B blocks and the inner A blocks form the matrix. The same notations are used for the gyroid and sphere phases.

To understand the formation mechanism of these two types of cylindrical phases in a star-like diblock copolymers, the density distributions of some special segments, including the

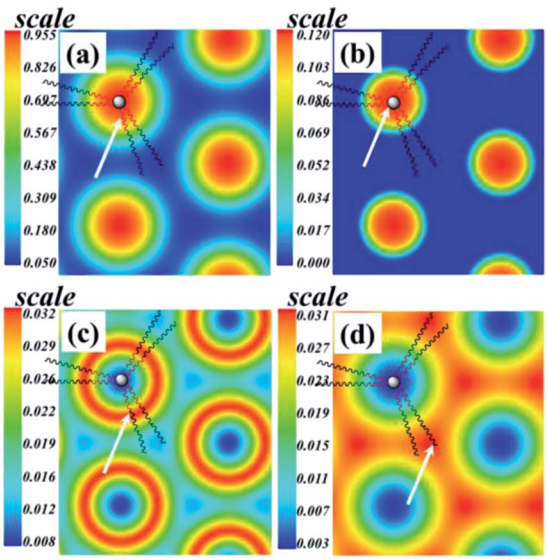

Fig. 2 Segment density distributions of normal cylindrical morphology from 21-arm star-like diblock copolymers ($\chi N = 250$ and $\phi_A = 0.35$). Density distribution of (a) the A blocks (deep red), (b) the core (deep red), which resembles the β-cyclodextrin (β-CD) core in ref. 12 and 13, (c) the junction points between A and B blocks (deep red), and (d) the chain end of B blocks (deep red). The white arrow in each figure marks these segments accordingly. Only six representative arms (not a total of 21 arms) are shown for the reason of clarity.

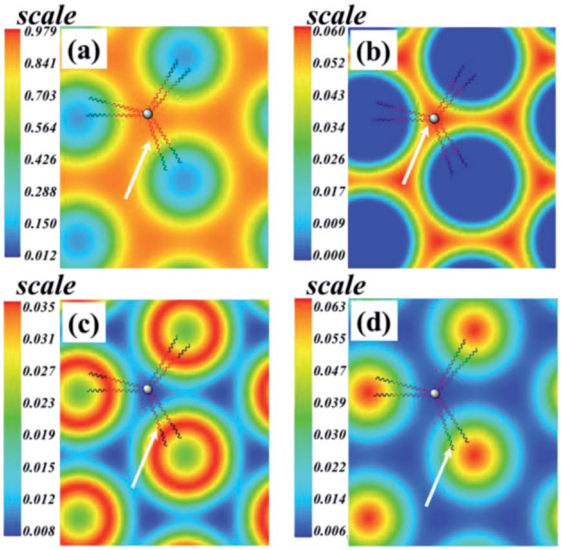

Fig. 3 Segment density distribution of inverse cylindrical morphology from the 21-arm star-like block copolymer ($\chi N = 250$ and $\phi_A = 0.65$). Density distribution of (a) the A blocks (deep red), (b) the core (deep red), which resembles the β-cyclodextrin (β-CD) core in ref. 12 and 13, (c) the junction points between A and B blocks (deep red), and (d) the chain end of B blocks (deep red). The white arrow in each figure marks the corresponding segment. Only six representative arms are shown for the reason of clarity.

core that connects 21 arms, the junction points between A and B block, and the chain end of B blocks are calculated and depicted in Fig. 2 and 3, which are otherwise difficult to be observed in experiment. The parameters chosen are $\chi N = 250$, $\phi_A = 0.35$. Compared with a linear diblock copolymer, the χN needed for the microphase separation to occur is very large due to the star-like architecture and the large number of arms. However, the star-like diblock copolymer has a large degree of polymerization,[11–13] thus a high χN can be easily realized.

The colored bars in each figure represent the densities of the corresponding special segments, ranging from the rich region (deep red) to the poor region (deep blue). The architecture of a 21-arm star-like block copolymer is also illustrated in each figure. As it is hard to place all 21 arms in the cylindrical morphology, only six representative arms are shown in each figure. The special segments in the 21-arm star-like diblock copolymer are indicated by the white arrows. Fig. 2a displays the density distribution of A blocks in the cylindrical morphology. The distribution of core that connects the 21 arms is shown in Fig. 2b, in which the core resembles the β-CD core in ref. 12 and 13. Clearly, the diameter of the core distribution is smaller than that of A block. The colored bar in Fig. 2a varies from 0.0503 to 0.955, while the highest density in Fig. 2b is only 0.12. This is not surprising as only the concentration of one special segment (*i.e.*, core) is depicted in Fig. 2b, while the concentration of the whole A block is illustrated in Fig. 2a. The distribution of the junction points between A and B blocks, which are located at the A block/B block interface, is shown in Fig. 2c. Fig. 2d describes the density distribution of the chain end of B blocks, which is located at the center of B blocks. From the density distribution of these special segments noted above, the arrangement of star-like diblock copolymers in the first type of cylindrical phase can be well understood.

For the second type of the cylindrical phase (*i.e.*, inverse cylinders), the distribution of these segments are expected to be quite different due to the packing frustration where the inner A blocks constitute the matrix. Such a packing frustration would lead to the largely different distributions of special segments as compared to those shown in Fig. 2. To investigate the formation of this frustrated cylindrical morphology, the distribution of the special segments of the inverse cylinders at $\chi N = 250$ and $\phi_A = 0.65$ was calculated and is shown in Fig. 3. Obviously, as the inner A blocks form the matrix, the distribution of the core dispersed in the A block (Fig. 3b) is completely different from that in Fig. 2b. Similar to the case of normal cylindrical morphology (Fig. 2c and d), the junction points between A and B blocks are located at the A block/B block interface, and the chain end of B blocks is centered in the B blocks (Fig. 3c and d).

Free energy and the corresponding periods of normal and inverse phases

For the inverse cylinders, because of the packing frustration, the free energy in this morphology is certainly larger than that in the normal cylinders. To gain a better understanding on this phase behavior, the free energy as a function of volume fraction at the fixed $\chi N = 250$ for different stable morphologies is calculated and summarized in Fig. 4a. The close-ups of dash-boxed regions in Fig. 4a are shown in Fig. 4b–d, respectively. As the volume fraction of the inner A blocks increases, the emergence of stable phases follows D → S → C → G → L → $\bar{G}$ → $\bar{C}$ → $\bar{S}$ → D. The order–order phase transitions (OOTs) between the neighboring phases are indicated by the arrows. For the disordered phase (*D*), which is the black curve with square symbols, the free energy curve is symmetric as there is only enthalpic energy in the disordered phase, and the free energy can be expressed as $F = \chi N\phi(1 - \phi)$. The free energy is only dependent on the volume fraction and χN, but independent on the polymer architectures. However, for the ordered phases (*i.e.*, lamellae, gyroid, cylinder, and sphere), the free energy curve is asymmetric. The S, C, and G without an overbar indicate the normal sphere, cylinder, and gyroid, respectively, where the outer B blocks form the matrix. The $\bar{S}$, $\bar{C}$, and $\bar{G}$ with an overbar imply the inverse morphologies, where the inner A blocks form the matrix because of the spontaneous curvature. Notably, the inverse morphologies have higher free energy than the normal morphologies (Fig. 4a). The region of the inverse phases becomes much narrower. The increase of free energy of inverse phases relative to the normal phases can be rationalized by the fact that it is energetically unfavorable for the inner A blocks to form the matrix, thus leading to the increase in stretching energy.

It is well known that the period of phases is closely related to the stretching of polymer chains,[29] which is clearly manifested in the period shown in Fig. 4e. In comparison to the normal

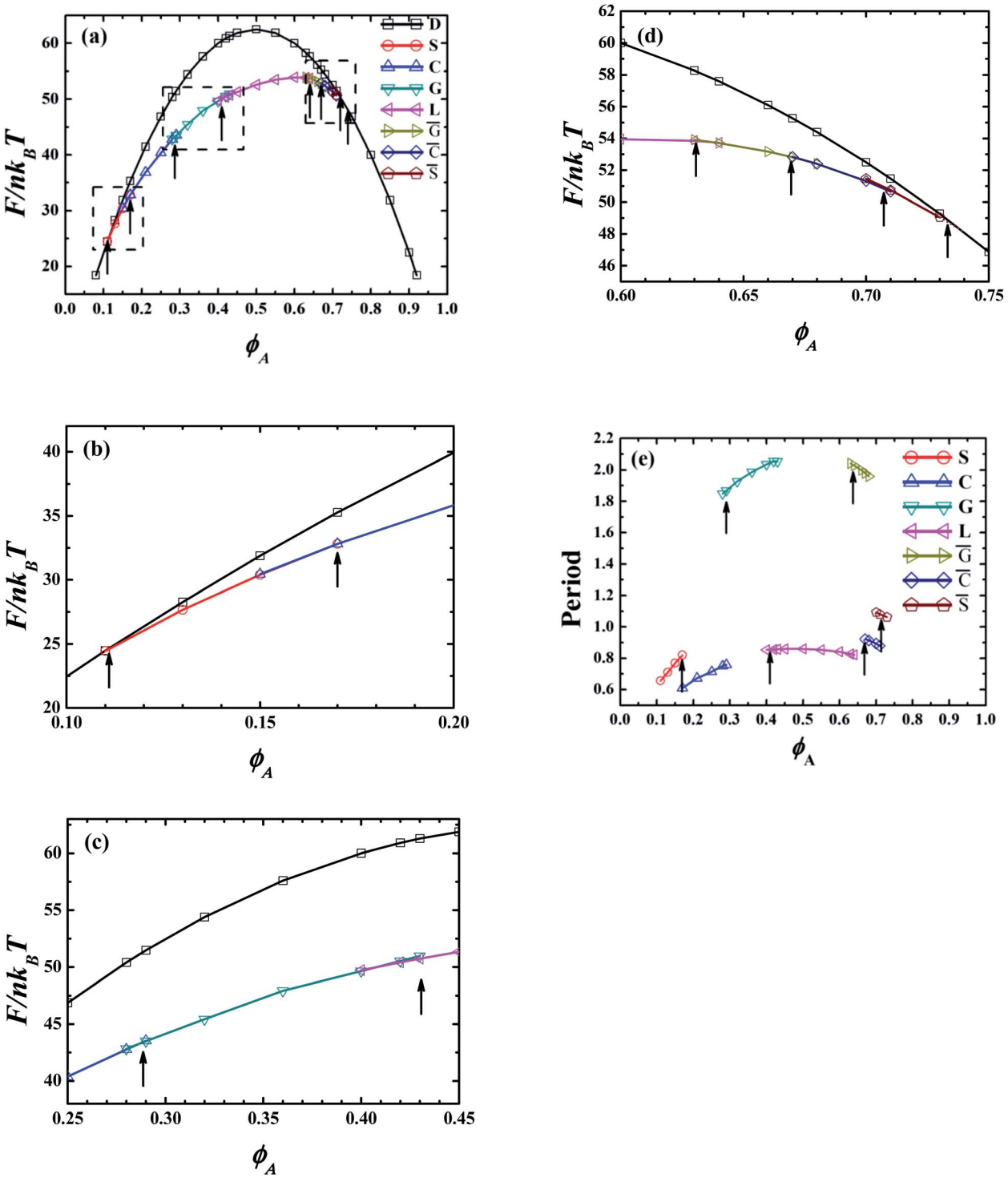

Fig. 4 (a) The free energy and (e) the corresponding period of different structures at different volume fractions with $\chi N = 250$. D, S, C, G and L denote phases of disordered, sphere, cylinder, gyroid, and lamella, respectively. An overbar in $\bar{G}$, $\bar{C}$, and $\bar{S}$ indicates the inverse morphologies of gyroid, cylinder, and sphere, respectively. The arrows indicate the order–order phase transitions between two neighboring phases. The close-ups of dash-boxed regions in (a) are shown in (b), (c), and (d), respectively.

phases, for the gyroid and lamellar phases, the periods of inverse phases do not change appreciably, indicating that polymer chain is not stretched too much in the inverse phases. For the spheres and cylinders, the inverse morphologies possess the larger period than the normal structures, signifying a large stretching of polymer chains in these inverse morphologies. Consequently, both the free energy and the period are increased.

The results noted above suggest that the star-like architecture is favorable for the formation of the normal morphologies.

When the volume fraction of inner A blocks is increased, they have to be stretched to form the matrix. The delicate balance between the topological constraint and the spontaneous curvature leads to the formation of inverse phases.

Phase diagram of a 21-arm star-like block copolymer

To gain further insight into the formation of each phase, the phase diagram of a 21-arm star-like diblock copolymer was calculated by comparing the free energy among possible candidate structures (Fig. 5). As we only focus on the influence of star-like architecture on the conventional morphologies (*i.e.*, S, C, G, and L), the O^{70}, A^{15} and perforated lamella are not considered in our calculation.[30] The degree of polymerization of the 21-arm star-like diblock copolymer is N, and thus, the degree of polymerization of each arm is $N/21$. To the best of our knowledge, there has been no experimental phase diagram of a 21-arm star-like block copolymer reported in literature to date. However, the lamellae morphology was found in the $(PS\text{-}b\text{-}PI)_{25}$ star-like block copolymer, where ϕ is 0.527.[11] It is anticipated that a lamellae morphology would form in the 21-arm star-like block copolymer at $\phi = 0.527$, which is located in the calculated L phase region in the present study. It is noteworthy that when compared to a linear diblock copolymer, the phase diagram is asymmetric,[8] which is consistent with the previous work on the phase diagram of a 9-arm star-like block copolymer.[9,30] The phase region of normal S, C, and G morphologies is larger than that of inverse $\bar{S}$, $\bar{C}$, and $\bar{G}$ morphologies, which is also in good agreement with the free energy calculations shown in Fig. 4a. The appearance of a larger phase region is attributed to the star-like architecture.

It is interesting to note that the $\bar{G}$ morphology was previously experimentally observed in the 18-arm star-like block copolymer and was regarded as an ordered bicontinuous double-diamond (OBDD) phase.[31,32] The phase behavior of 18-arm block copolymers is similar to that of 21-arm block copolymers in this study, indicating that the $\bar{G}$ morphology obtained experimentally was in a very narrow phase region.[31,32] The formation of $\bar{G}$ benefits from the close period between the G and $\bar{G}$ morphologies (Fig. 4b). On the basis of the phase diagram of the 21-arm star-like diblock copolymer, it can be anticipated that the formation of G would become much easier in the 18-arm star-like block copolymer if the inner block has a small volume fraction and is located at the G phase region. Specifically, the O^{70}, which is not observed in our calculations because this structure is sensitive to the chosen parameters (*i.e.*, box size), can be expected to form in the region where the inner block has a small volume fraction. More importantly, the disordered phase has a large phase region (Fig. 5), implying that the microphase separation in star-like diblock copolymers is more difficult than that in linear diblock copolymers with the same N. In particular, when the inner A blocks have a large volume fraction, the microphase separation becomes much harder. This can be ascribed to the fact that the high free energy of inverse morphology results in the formation of the disordered morphology.

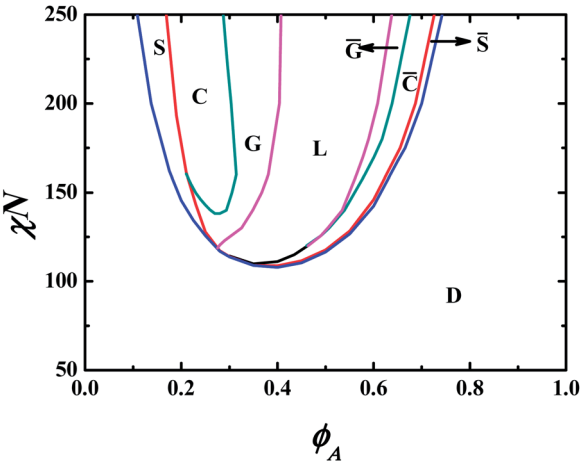

Fig. 5 The phase diagram of a 21-arm star-like diblock copolymer. N is the total degree of polymerization of the star-like diblock copolymer, and thus, the degree of polymerization of each arm is $N/21$. The disordered phase is labeled as D. The normal ordered phases are labeled as S (spheres), C (cylinders), G (gyroids), and L (lamellae). The G, C, and S with an overbar represent the inverse phases.

Bridging fraction in the 21-arm star-like diblock copolymer

It has been reported that in the morphologies formed from ABA triblock copolymers, there are looped and bridged configurations.[15] Although these configurations have little effect on the equilibrium phase behavior, the mechanical properties of materials are strongly affected by the presence of bridges as the separated interfaces can be covalently linked together. For the multi-arm system, the bridging fraction would increase with the increase in the number of arms. In what follows, we concentrate on the calculation of the bridging fraction in multi-arm star-like diblock copolymers.

According to the previous studies,[15,33] we constrained one junction point to a unit cell and then calculated the probability of one of the other junction points forming the loop configuration. As one of the junction points is fixed at a region, we have

$$q(\mathbf{r}, f_{C1}) = \begin{cases} q(\mathbf{r}, f_{C1}), & \text{if } \mathbf{r} \in \text{1st cell} \\ 0, & \text{otherwise} \end{cases} \quad (17)$$

where f_{C1} is the segment of one junction point constrained to the first unit cell. Once this initial condition is determined, the distribution of the whole chain can be obtained by solving the modified diffusion equation (eqn (6)). Then, the distribution of the ith junction point with one junction point in the first unit cell can be achieved by using the following equation.

$$\rho(\mathbf{r}, s_{Ci}) = \frac{1}{Q} q(\mathbf{r}, s_{Ci}) q^{\dagger}(r, s_{Ci}), \quad (18)$$

where s_{Ci} is the ith junction point, and $i \neq 1$.

When the other junction is also in the first unit cell, the loop configuration is formed. Thus, the fraction of the looped configuration can be given as

$$f_{lp1} = \frac{1}{V_{cell}} \int_{1st\ cell} dr\rho(r, s_{Ci}) \quad (19)$$

where V_{cell} is the volume of a unit cell. The bridging fraction is defined as $f_{br} = 1 - (f_{lp1})^{f-1}$ where f is the number of arms. Fig. 6 shows the bridging fraction in a lamellar morphology as a function of f. It is clearly evident that the bridging fraction in 21-arm star-like diblock copolymers is almost 100%, making it a promising candidate for a wide variety of potential applications (*e.g.*, thermoplastic elastomers).

Self-assembly under cylindrical confinement

Compared to the variation of the chemical compositions, the architectures, or the interactions between immiscible blocks in block copolymers, the introduction of geometric confinement has been recognized as an alternative approach to fabricating novel ordered nanostructures. In the following, we turn our attention to the self-assembly of 21-arm star-like block copolymers under cylindrical confinement (*i.e.*, cylindrical nanopores) for the first time.

According to previous work,[20–22,34,35] the use of confinement on the cylinder-forming block copolymer in bulk leads to the creation of many intriguing morphologies. In this work, we chose the volume fraction of a 21-arm star-like block copolymer, $\phi_A = 0.2$, and $\chi N = 250$, which can be readily obtained in the experiment by controlling the monomer concentration of different blocks.[12] In bulk, such a star-like diblock copolymer forms hexagonally close-packed cylinders composed of the A blocks with a spacing of $L_0 = 0.743R_g$ between the center–center distance of two neighboring cylinders. The strength of the surface field is chosen as $V_0 = -0.20$ to exert a strong attraction to the outer B blocks and a strong repulsion to the inner A blocks.

For a 21-arm star-like diblock copolymer confined in cylindrical nanopores, many equilibrium solutions of the SCMFT equations at the fixed set of parameters in the 2D space can be obtained by the application of varied random initial fields. The stability of each structure as well as their stable phase sequence as a function of the pore size can be identified by comparing its free energy with other candidate structures. The stable and metastable 2D structures and their phase sequence are summarized in Fig. 7a and b, respectively. The complexity of the phases, reflected in both the number of cylinders and rings, increases as the pore diameter increases. The 2D phase sequence, $C_1 \rightarrow C_3 \rightarrow C_4 \rightarrow C_{1-6} \rightarrow C_{1-8}$, is consistent with that of the linear diblock copolymer in the cylindrical confinement, $C_1 \rightarrow C_3 \rightarrow C_4 \rightarrow C_5 \rightarrow C_{1-6} \rightarrow C_{1-8}$.[21] Because of the restriction of the star-like architecture, some phases such as C_5 cannot be observed. The L_1 morphology, which does not appear in the stable phase sequence, is a metastable phase in which the arrangement becomes more frustrated due to the compression of large outer B blocks in the core of nanopore.

Similar to the self-assembly of linear diblock copolymers under cylindrical confinement, there is another possible way for star-like copolymers to produce microphases. The star-like diblock copolymer chain tries to release its stretching through the third dimension, thereby leading to the formation of three-dimensional phases, such as the helix phase. By inputting a large number of random initial conditions, we only obtained the double helix phase (H_2) from the 3D SCMFT calculation under this condition. This further demonstrates that the phase separation of 21-arm star-like diblock copolymers is harder than that of linear diblock copolymers because of the restriction of the star-like architecture. The isosurface density plot of H_2 and the comparison of the free energy of new stable phase sequences are shown in Fig. 8. For the reason of clarity, a free energy difference, ΔF, defined as the value of the free energy of a morphology subtracted by that of H_2, is used to identify the relative stability among these morphologies. As evidenced in Fig. 8, the 3D structure has a lower free energy than the corresponding 2D structures shown in Fig. 7. This can be attributed to the release of polymer stretching in the third dimension in 3D phases. In addition, the free energy difference has a decreased tendency with the increase of pore size. Notably, this observation is consistent with the results of ABC star triblock copolymers under cylindrical confinement.[22]

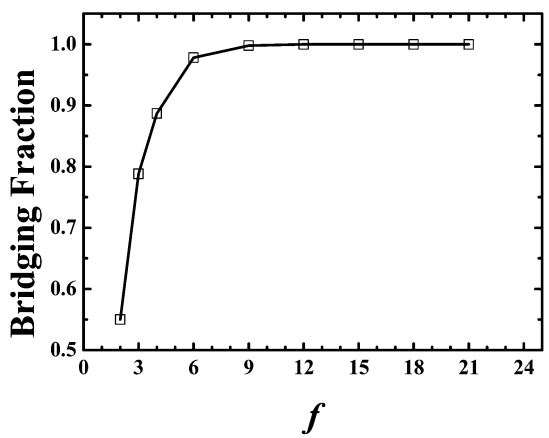

Fig. 6 The bridging fraction plotted as a function of the number of arms, f. The $\chi N/f$ is fixed at 10 for this 21-arm star-like diblock copolymer.

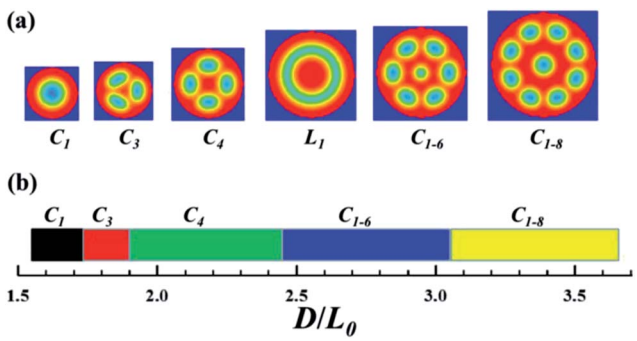

Fig. 7 (a) Density plots of the stable and metastable morphologies formed in the cylinder-forming 21-arm star-like diblock copolymer at $\phi_A = 0.2$, $\chi N = 250$, and $V_0 = -0.20$, under the cylindrical confinement with the varied diameter (D) of nanopores, normalized by the bulk cylinder-to-cylinder distance, $L_0 = 0.743R_g$. (b) Stable phase sequence of the morphologies as a function of D/L_0.

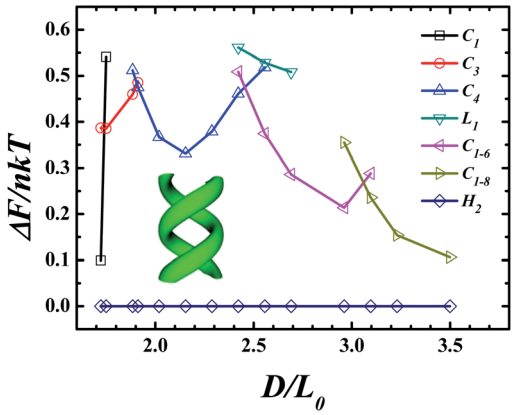

Fig. 8 Comparison of the free energy between two-dimensional structures and three-dimensional structures with the varied pore size. For clarity, the free energy relative to that of double helix (H_2) is shown in the figure. The inset gives the isosurface density plot of H_2.

Conclusions

In summary, the phase behavior of a 21-arm star-like diblock copolymer in bulk and under cylindrical confinement was explored by using real space SCMFT. In comparison with a linear diblock copolymer of the same N, a larger χN is needed for the microphase separation of a 21-arm star-like diblock copolymer. An asymmetric phase diagram was constructed by comparing the free energy of different structures. The inverse morphologies exhibit a narrow phase region because of the frustration between the inverse morphology and the star-like architecture. In particular, the normal gyroid possesses a large phase region when the inner block in star-like diblock copolymer has a small volume fraction, suggesting the propensity to form the gyroid under this condition. In addition, a scaling law correlating the period, $D_{\text{multiarms}}$, with the number of arms f, $D_{\text{multiarms}} = D/f^{1/2}$, was identified. The bridging fraction of the lamellae formed in the star-like diblock copolymer was nearly 100%, offering improved mechanical properties. Some interesting two-dimensional and three-dimensional morphologies were produced under the cylindrical confinement. The 2D phase diagram suggested that the phase sequence is consistent with that of a linear diblock copolymer under the cylindrical confinement. Moreover, instead of a 2D structure, a 3D double helix, in which the star-like diblock copolymer chain tends to release its stretching energy in the third dimension, became more stable.

Acknowledgements

We gratefully acknowledge funding support from National Natural Science Foundation of China (Grants 21304051 and 21322407), K. C. Wong Magna Foundation at Ningbo University, National Science Foundation (NSF CBET-1159048), and Air Force office of Scientific Research (MURI FA9550-14-1-0037).

Notes and references

1 K. Char, C. W. Frank and A. P. Gast, *Langmuir*, 1989, **5**, 1335.
2 K. Char, C. W. Frank and A. P. Gast, *Langmuir*, 1989, **5**, 1096.
3 K. Char, C. W. Frank and A. P. Gast, *Macromolecules*, 1989, **22**, 3177.
4 B. J. de Gans, S. Wiegand, E. R. Zubarev and S. I. Stupp, *J. Phys. Chem. B*, 2002, **106**, 9730.
5 M. O. Delacruz and I. C. Sanchez, *Macromolecules*, 1986, **19**, 2501.
6 P. G. de Gennes, *J. Phys.*, 1970, **31**, 325.
7 E. Helfand, *Macromolecules*, 1975, **8**, 552.
8 M. W. Matsen and M. Schick, *Phys. Rev. Lett.*, 1994, **72**, 2660.
9 M. W. Matsen and M. Schick, *Macromolecules*, 1994, **27**, 6761.
10 Y. Xu, J. Feng, H. Liu and Y. Hu, *Mol. Simul.*, 2006, **32**, 375.
11 S. Uchida, A. Ichimura and K. Ishizu, *Polymer*, 1999, **40**, 1019.
12 X. C. Pang, L. Zhao, M. Akinc, J. K. Kim and Z. Q. Lin, *Macromolecules*, 2011, **44**, 3746.
13 X. C. Pang, L. Zhao, C. W. Feng and Z. Q. Lin, *Macromolecules*, 2011, **44**, 7176.
14 X. C. Pang, L. Zhao, W. Han, X. K. Xin and Z. Q. Lin, *Nat. Nanotechnol.*, 2013, **8**, 426.
15 M. W. Matsen and R. B. Thompson, *J. Chem. Phys.*, 1999, **111**, 7139.
16 S. F. Edwards, *Proc. Phys. Soc., London*, 1965, **85**, 613.
17 E. Helfand, *J. Chem. Phys.*, 1975, **62**, 999.
18 G. H. Fredrickson, *The equilibrium theory of inhomogeneous polymers*, Oxford University Press, Oxford, U. K., 2006.
19 A. C. Shi, *Development in block copolymer science and technology*, New York, 2004.
20 W. H. Li and R. A. Wickham, *Macromolecules*, 2006, **39**, 8492.
21 W. H. Li, R. A. Wickham and R. A. Garbary, *Macromolecules*, 2006, **39**, 806.
22 Y. C. Xu, W. H. Li, F. Qiu and Y. L. Yang, *J. Phys. Chem. B*, 2009, **113**, 11153.
23 W. Li and R. A. Wickham, *Macromolecules*, 2009, **42**, 7530.
24 G. Tzeremes, K. O. Rasmussen, T. Lookman and A. Saxena, *Phys. Rev. E*, 2002, **65**, 041806.
25 K. O. Rasmussen and G. Kalosakas, *J. Polym. Sci., Part B: Polym. Phys.*, 2002, **40**, 1777.
26 M. Rubinstein, *Polymer Physics*, Oxford, 2003.
27 A. N. Semenov, *Zhurnal Eksperimentalnoi I Teoreticheskoi Fiziki*, 1985, **88**, 1242.
28 M. W. Matsen, *J. Phys.: Condens. Matter*, 2002, **14**, R21.
29 Y. C. Xu, W. H. Li, F. Qiu, H. D. Zhang, Y. L. Yang and A. C. Shi, *J. Polym. Sci., Part B: Polym. Phys.*, 2010, **48**, 1101.
30 M. W. Matsen, *Macromolecules*, 2012, **45**, 2161.
31 E. L. Thomas, D. B. Alward, D. J. Kinning, D. C. Martin, D. L. Handlin and L. J. Fetters, *Macromolecules*, 1986, **19**, 2197.
32 D. A. Hajduk, P. E. Harper, S. M. Gruner, C. C. Honeker, E. L. Thomas and L. J. Fetters, *Macromolecules*, 1995, **28**, 2570.
33 F. Drolet and G. H. Fredrickson, *Macromolecules*, 2001, **34**, 5317.
34 Y. C. Xu, W. H. Li, F. Qiu, Y. L. Yang and A. C. Shi, *Phys. Chem. Chem. Phys.*, 2011, **13**, 12421.
35 B. Yu, P. C. Sun, T. H. Chen, Q. H. Jin, D. T. Ding, B. H. Li and A. C. Shi, *Phys. Rev. Lett.*, 2006, **96**, 138306.